On the enhanced coronal mass ejection detection rate since the solar cycle 23 polar field reversal

ApJ 812, 74

Gordon Petrie

NSO, Boulder, Colorado, USA

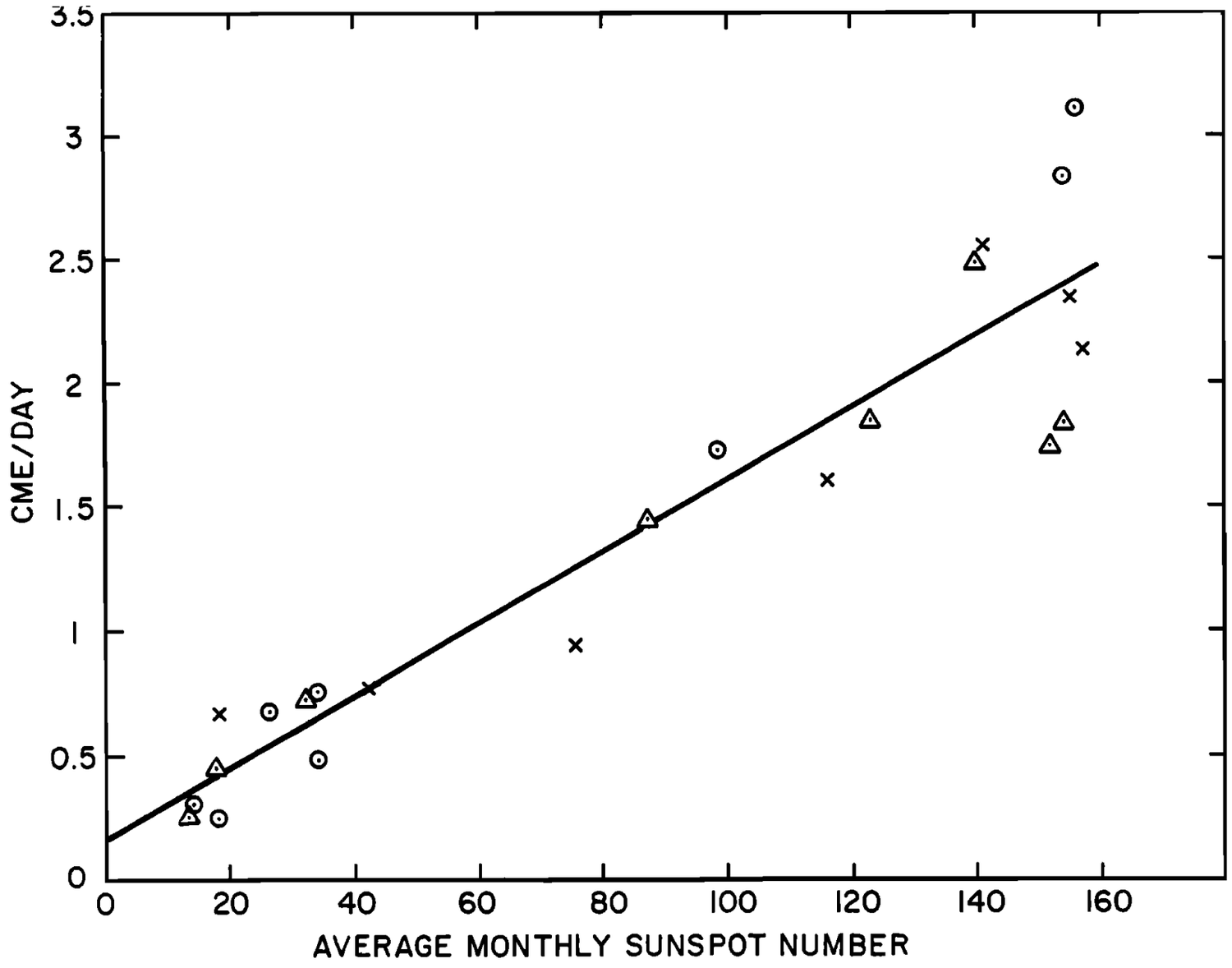

CME rate well correlated with activity cycle during 1975-1989.

Left: CME rate vs. average sunspot number for 1975-1989. The line is the linear regression fit, and the correlation coefficient is 0.94. The symbols represent the various CME data sources used.

From Webb & Howard (1994).

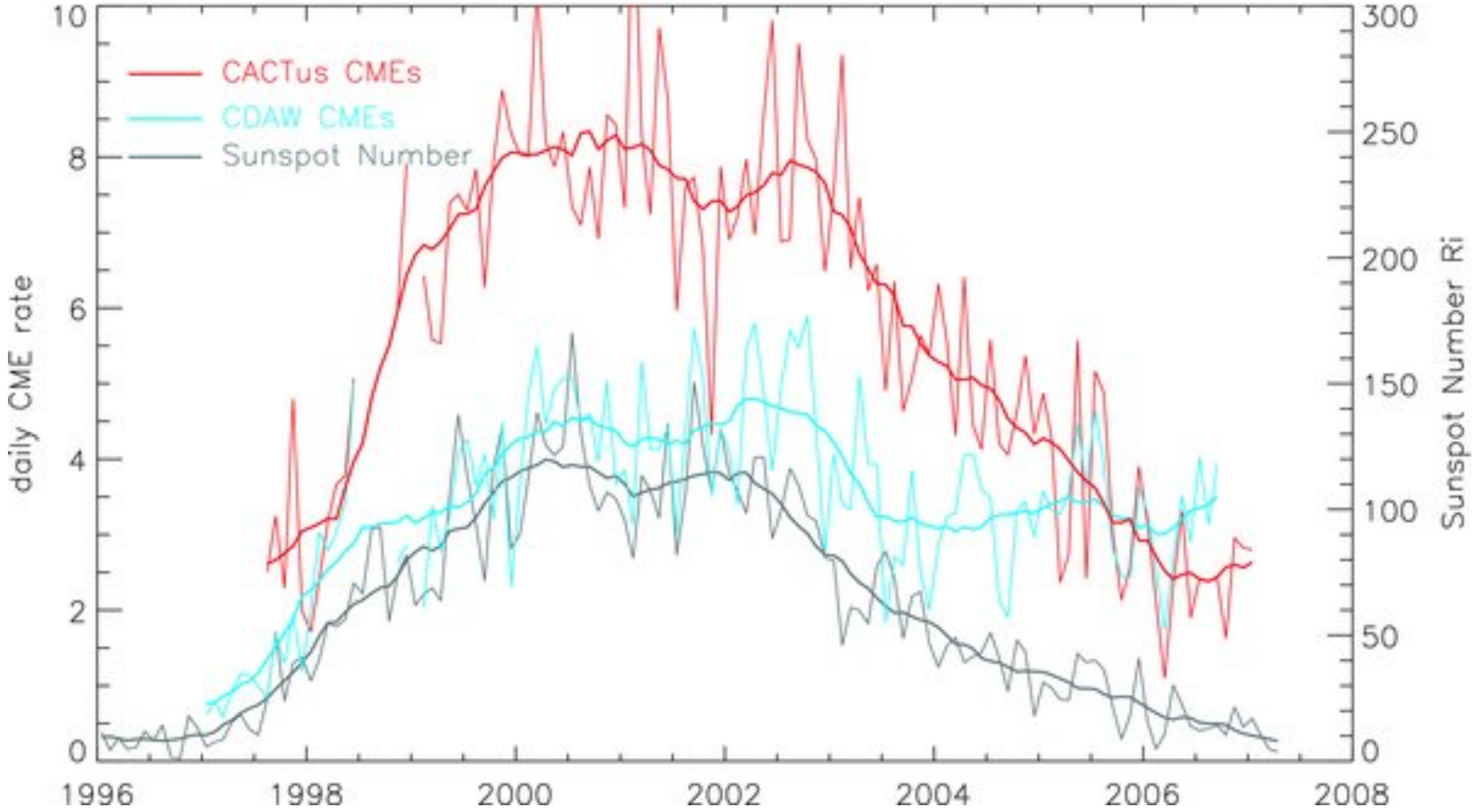

Cycle 23: CME rate lagged sunspot cycle by 6 months to a year.

Daily *SOHO* LASCO CME rates (thin curves: smoothed per month, thick curves: smoothed over 13 months) from 1997 to 2006, from the CACTus (red) and the CDAW (blue) CME catalog, with daily and monthly smoothed sunspot number overplotted in grey. From Robbrecht et al. (2009).

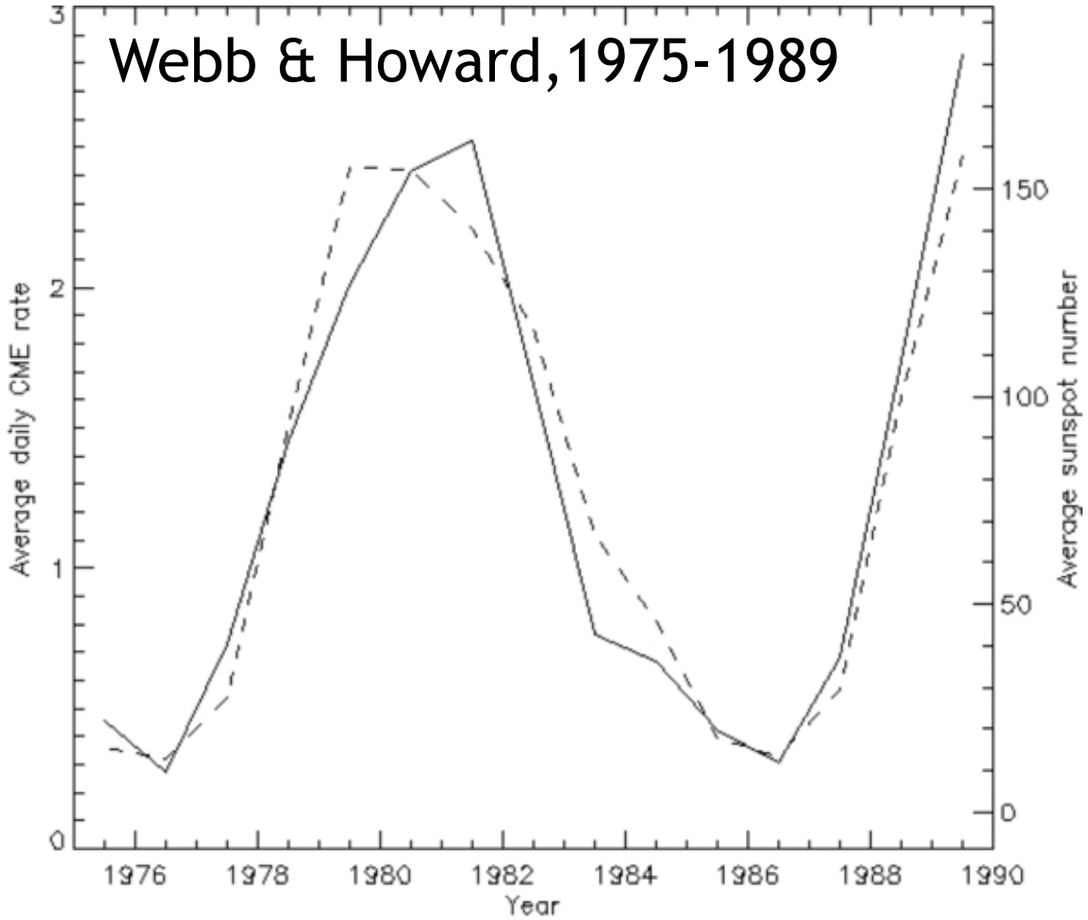

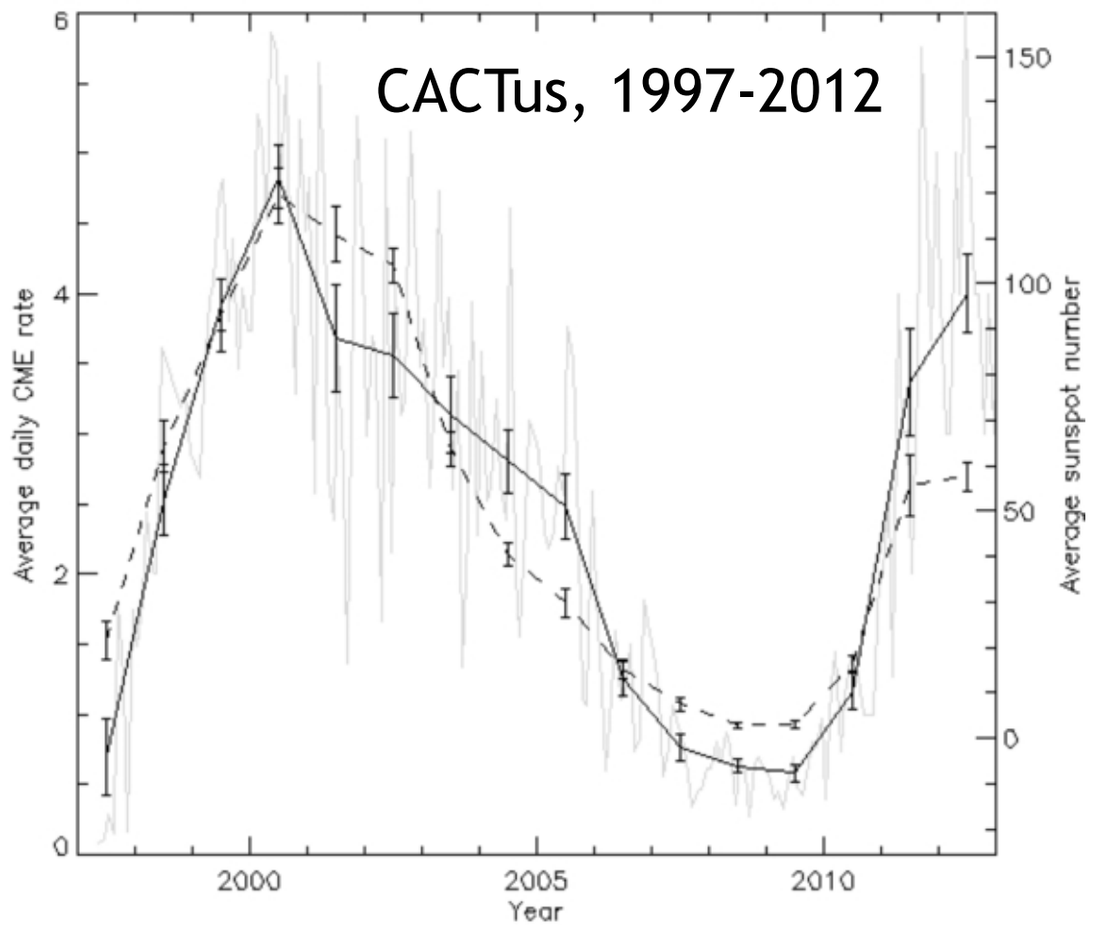

Change of behavior linked to polar fields?

Average daily CME rate for 1975-89 based on the data collected by Webb & Howard (1994, top left), and the annual (black solid lines) and for 1997-2012 according to CACTus (top right) and SEEDS (bottom). The averages sunspot number is over-plotted (black dashed lines) for comparison.

From Petrie (2013).

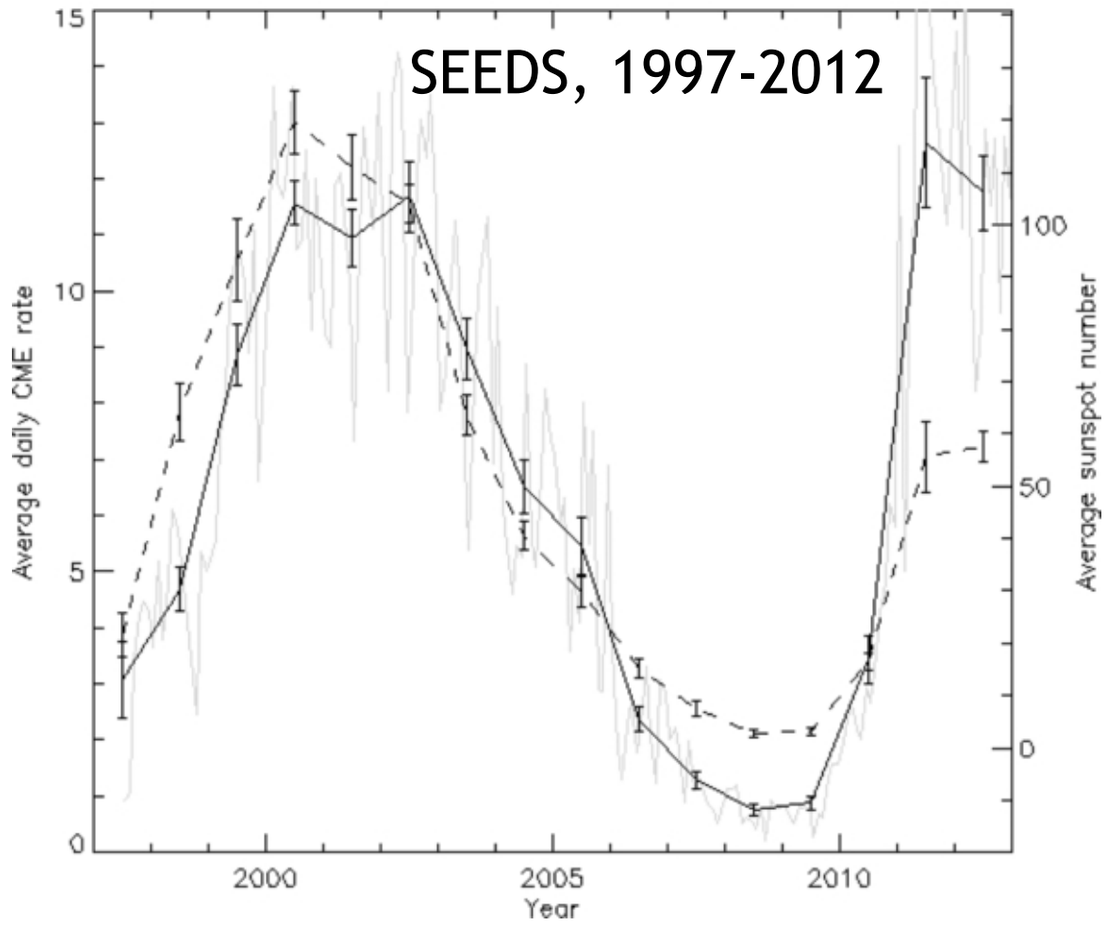

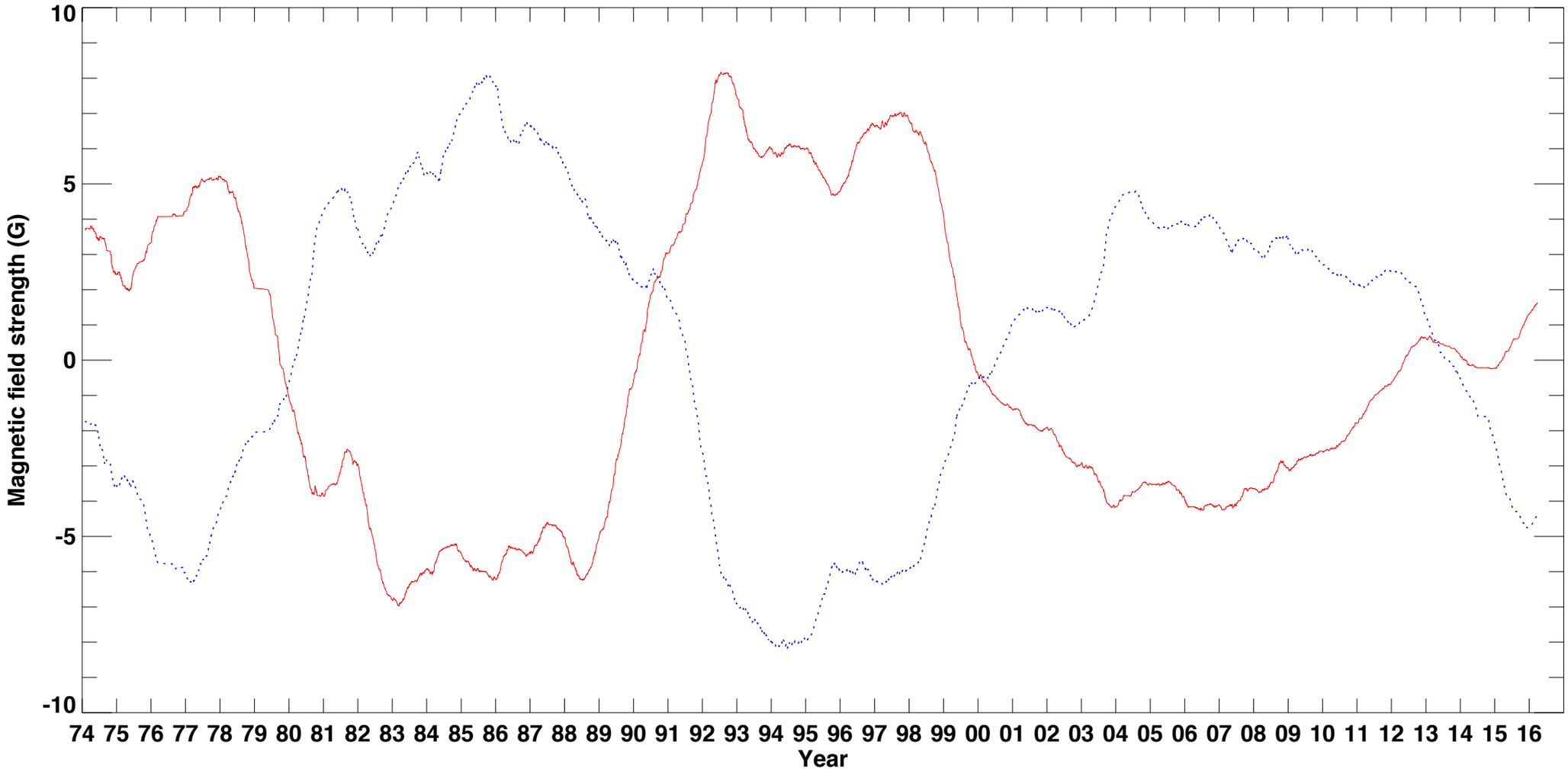

27-day averages of the north (red solid lines) and south (blue dotted lines) polar fields measured by the Kitt Peak Vacuum Telescope and the SOLIS/VSM. The measurements derive from heliographic latitudes ranging from ±63° to ±70°. Updated from Petrie (2013).

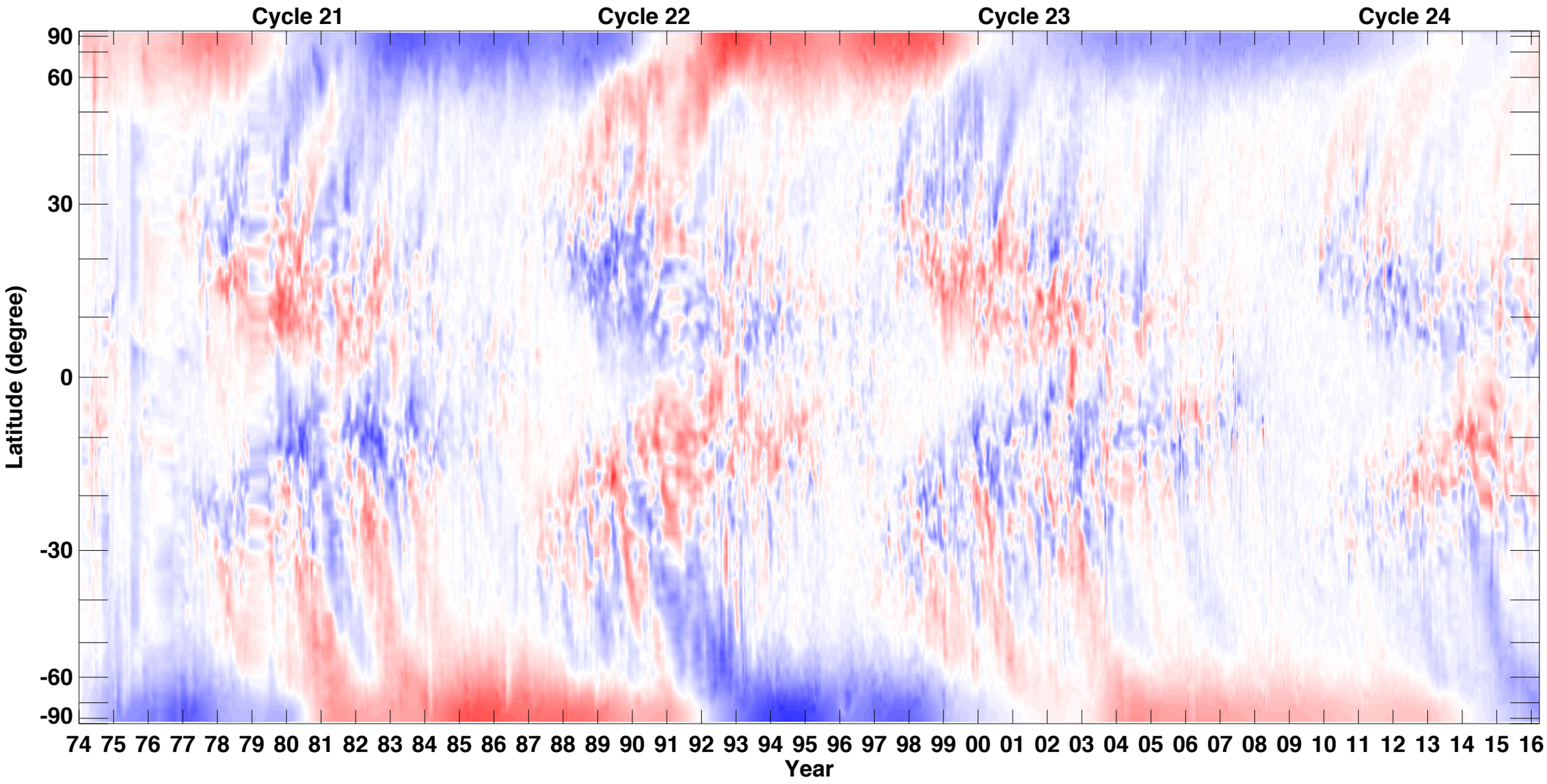

Butterfly diagram of NSO KPVT & SOLIS/VSM field measurements (1974-present, bad images filtered out). Red=positive, blue negative, saturates at ±15G.
Flux is transported from active latitudes to poles in unipolar surges. Polar fields respond to these surges.
Polar reversals can be fast/strong (cycle 21, 22, 24 S) or slow/weak (cycle 23, 24 N).
Cycle 23 polar fields' growth stunted around 2003-04 (Petrie 2012, 2015, Jiang et al. 2015).

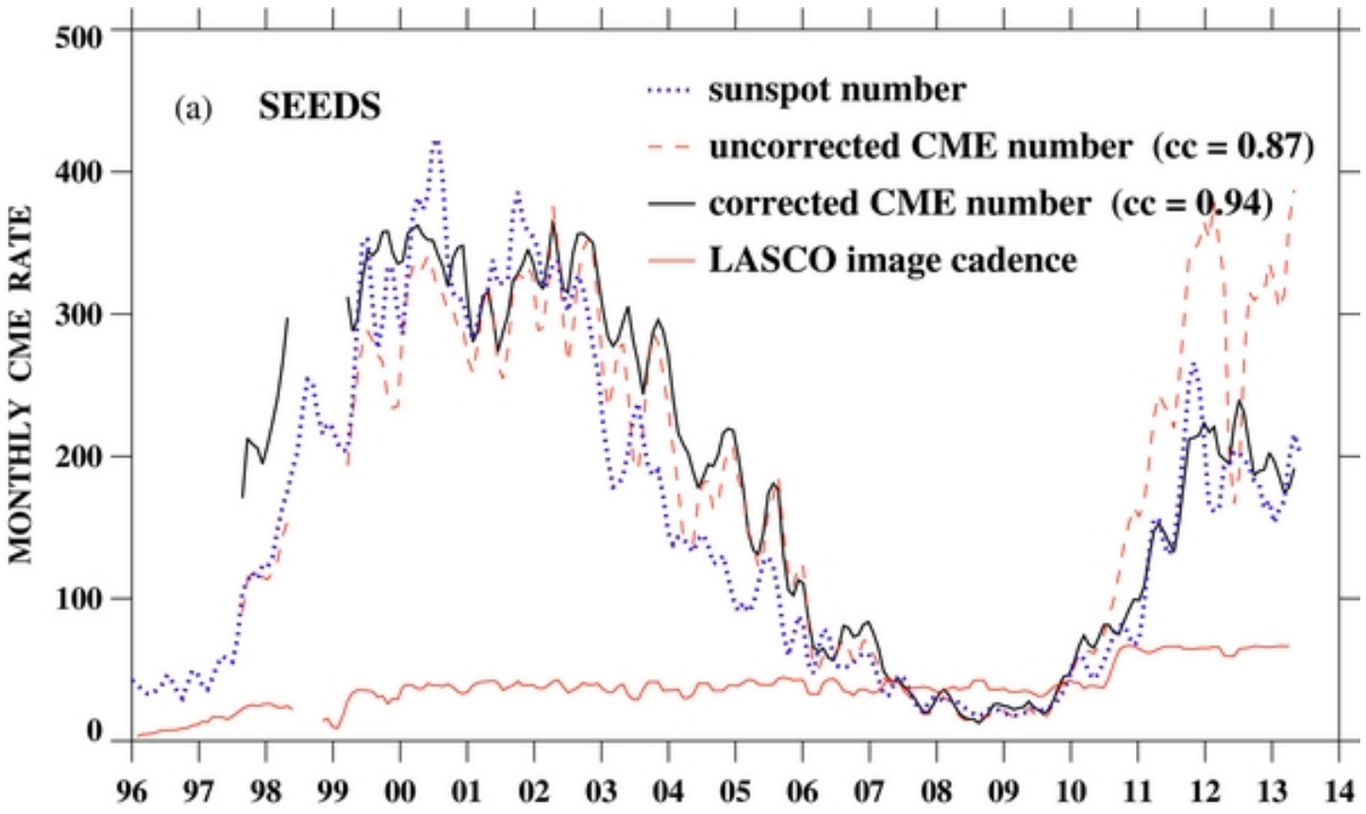

Change of behavior linked to LASCO image cadence change?

(a) Black curve: SEEDS CME rate, after correction by dividing by the LASCO C2 image cadence (solid red curve). Red dashed curve shows the original rate.

From Wang & Colannino (2014)

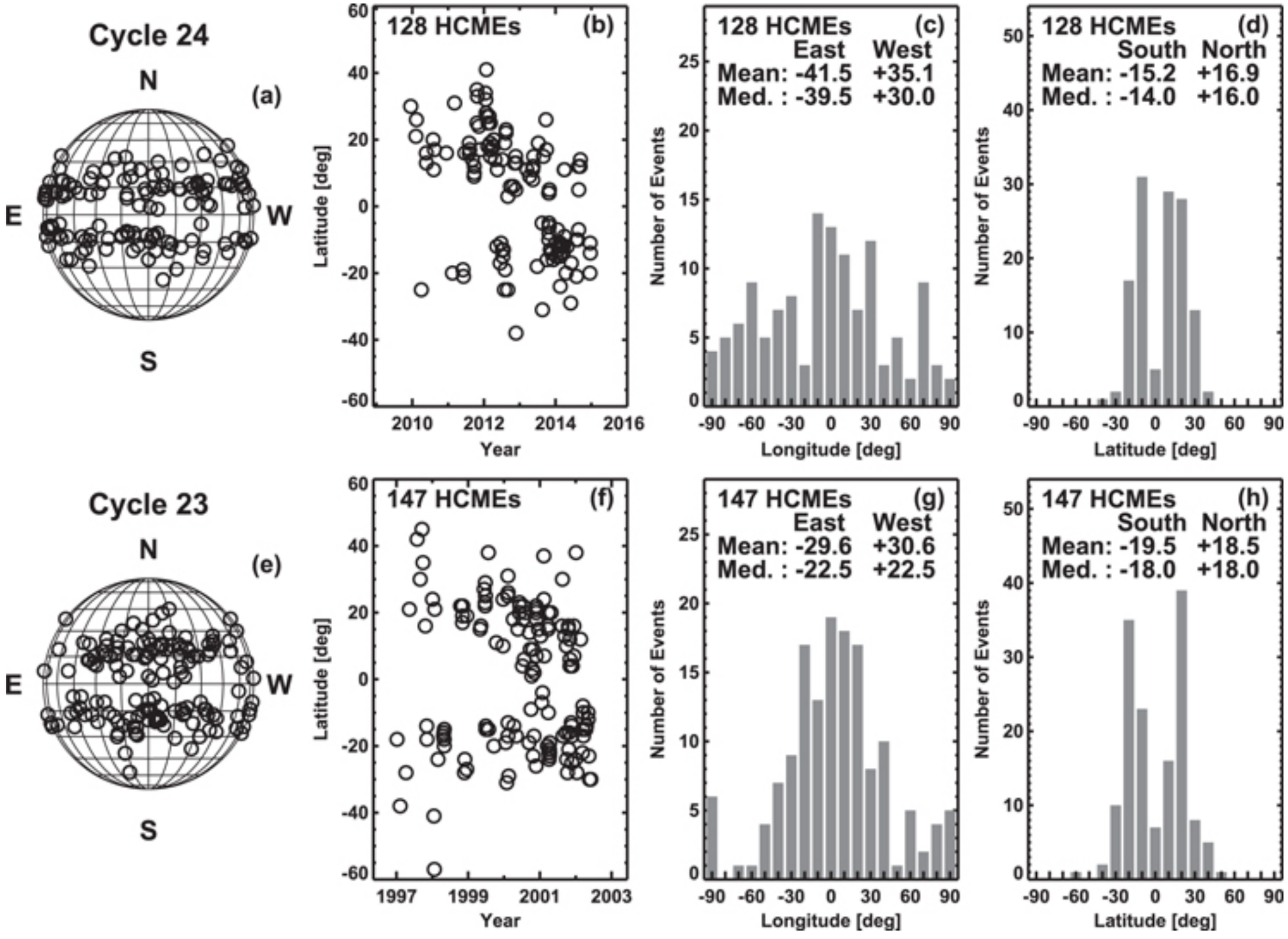

But halo CMEs show real change of behavior.

Comparison between halo CMEs of cycles 23 and 24.

Heliographic coordinates (a) and (e) and the solar-cycle variation of source latitudes (b) and (f), source longitudes (c) and (g), and source latitudes (d) and (h) of halo CMEs in cycles 24 (top row) and 23 (bottom row). The mean and median values are shown on the plots separately for each hemisphere (eastern and western for longitudes; southern and northern for latitudes). From Gopalswamy et al. (2015).

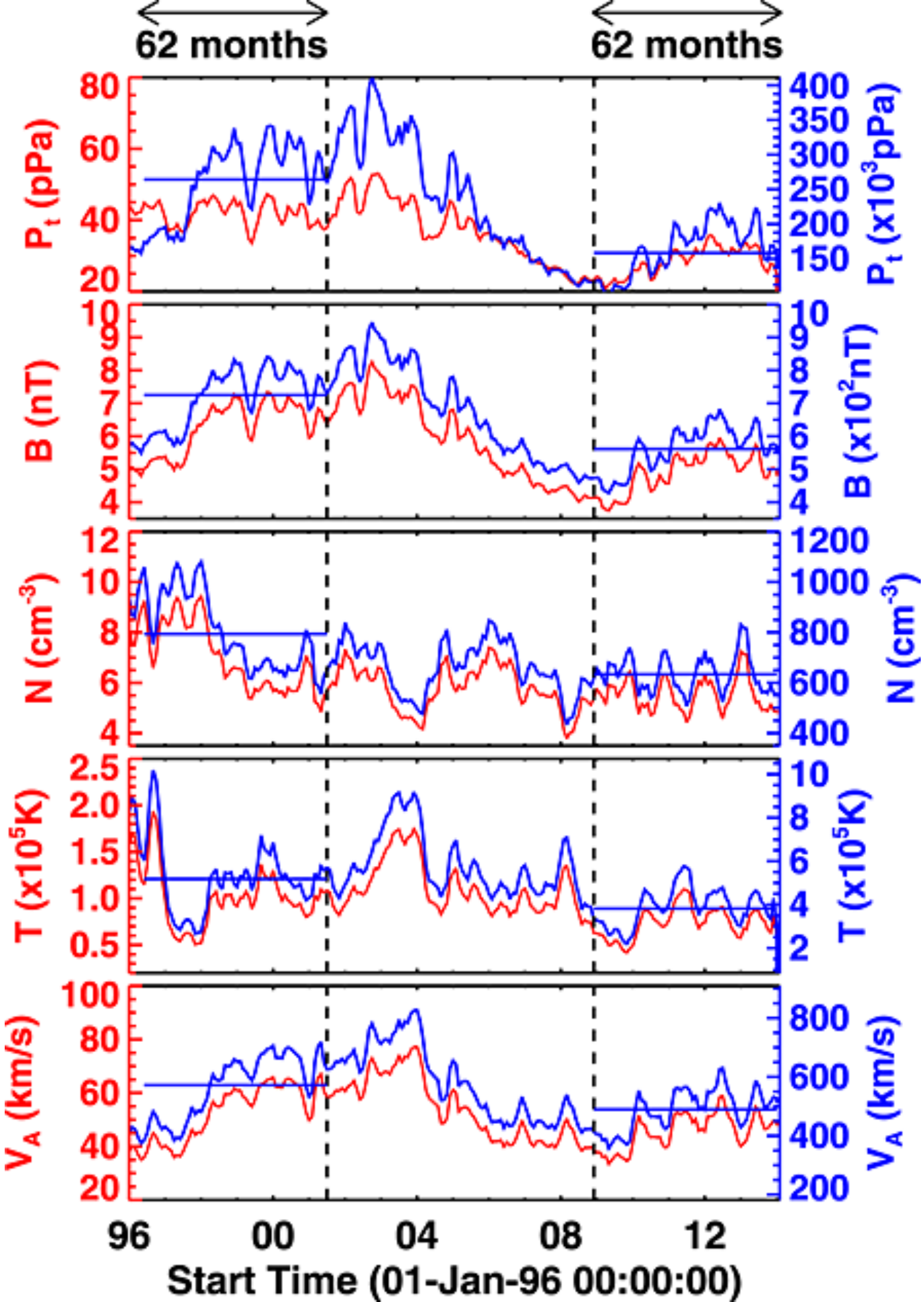

Total pressure (P_t), magnetic field magnitude (B), proton density (N), proton temperature (T), and the Alfvén speed (V_A) at 1 AU obtained from OMNI data (red lines with left-side Y axis). The same quantities extrapolated from 1 AU to the coronagraph FOV (20 R_S) are shown by blue lines (right-side Y axis), assuming that B, N, and T vary with the heliocentric distance R as R^{-2}, R^{-2}, and $R^{-0.7}$, respectively. The blue bars denote the 62 month averages in each panel, showing the decrease of all the parameters in cycle 24.

From Gopalswamy et al. (2014).

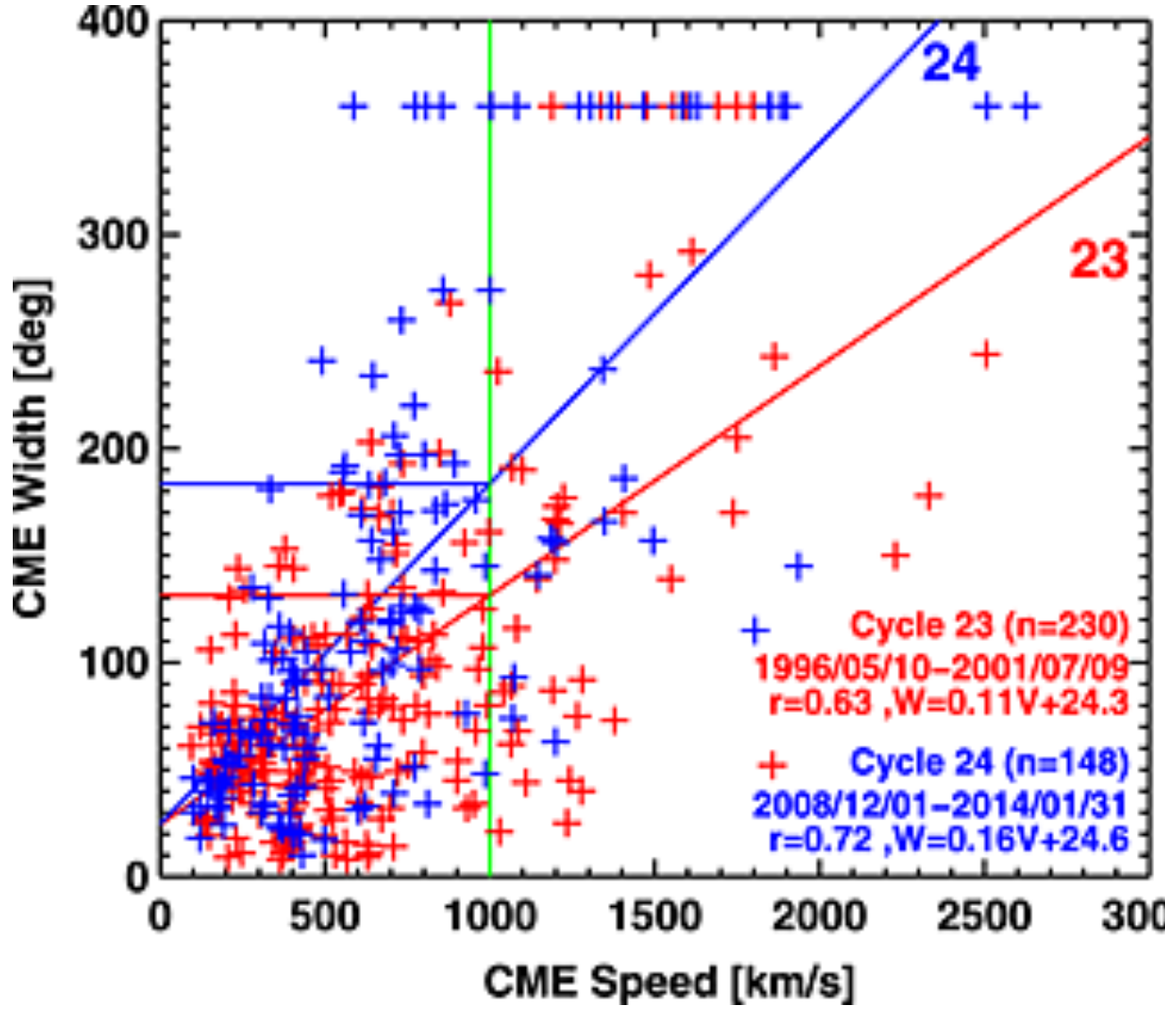

Scatter plots between CME speed (*V*) and angular width (*W*) for cycles 23 (red) and 24 (blue). The regression lines and the correlation coefficients are indicated on the plot. Note the width difference between the two cycles, e.g., at 1000 km/s (green line). From Gopalswamy et al. (2014).

Compare three online CME databases:

- the Coordinated Data Analysis Workshop (CDAW, http://cdaw.gsfc.nasa.gov, Gopalswamy et al. 2009),
- the Solar Eruptive Events Data System (SEEDS, http://spaceweather.gmu.edu/seeds/lasco.php, Olmedo et al. 2008),
- and the Computer Aided CME Tracking (CACTus, http://sidc.oma.be/cactus/, Robbrecht et al. 2009).

They have recorded CMEs over the LASCO era (1997-present).

The CDAW team identify CMEs by visual inspection of the LASCO C2 and C3 coronagraph images, whereas SEEDS and CACTus apply automated algorithms to identify CMEs without human intervention.

SEEDS uses C2 images alone, and CACTus and CDAW use images from both C2 and C3.

LASCO C2

LASCO C3

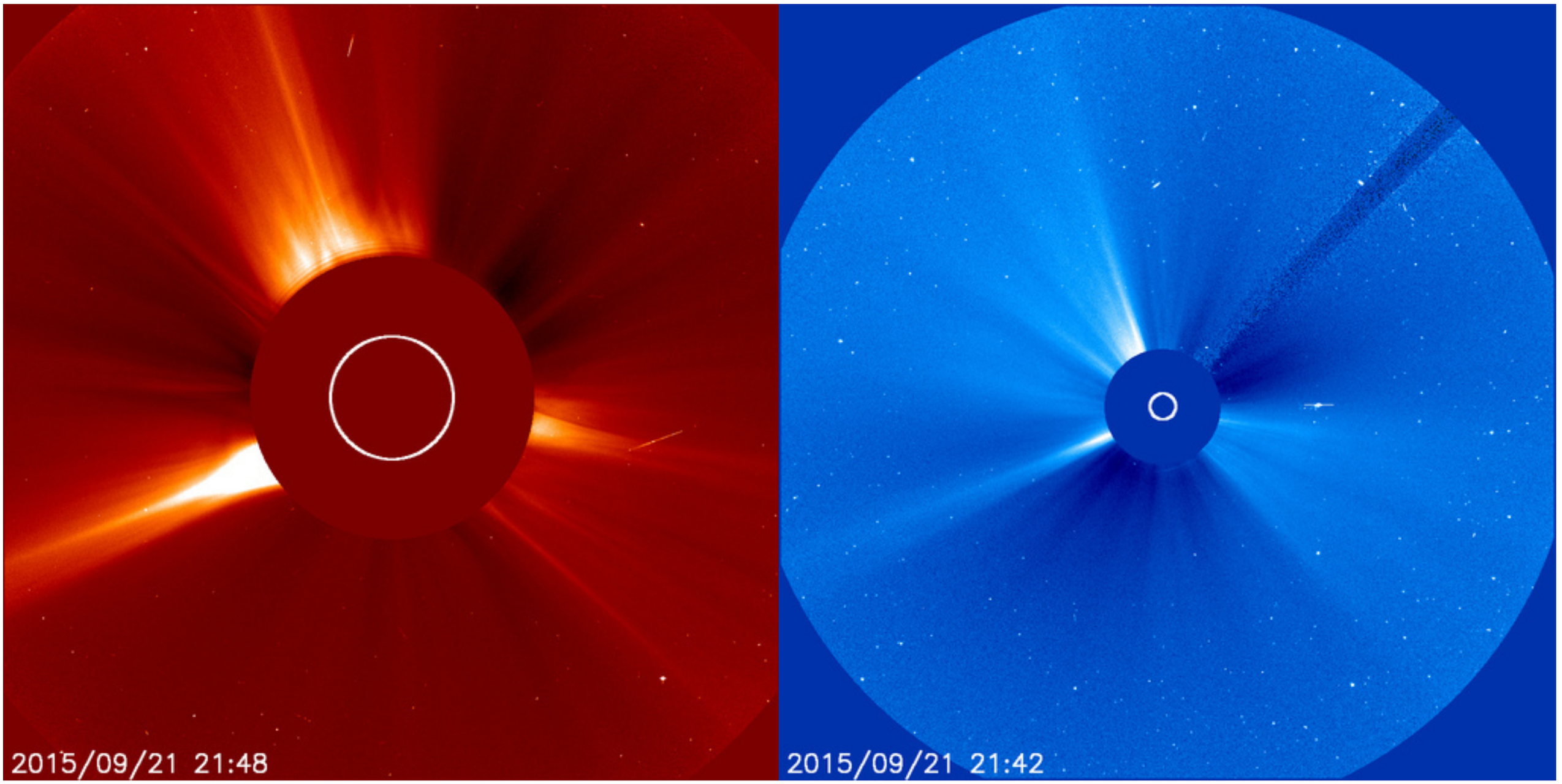

Field of view: 2-6 R_{Sun}

Field of view: 3.7-32 R_{Sun}

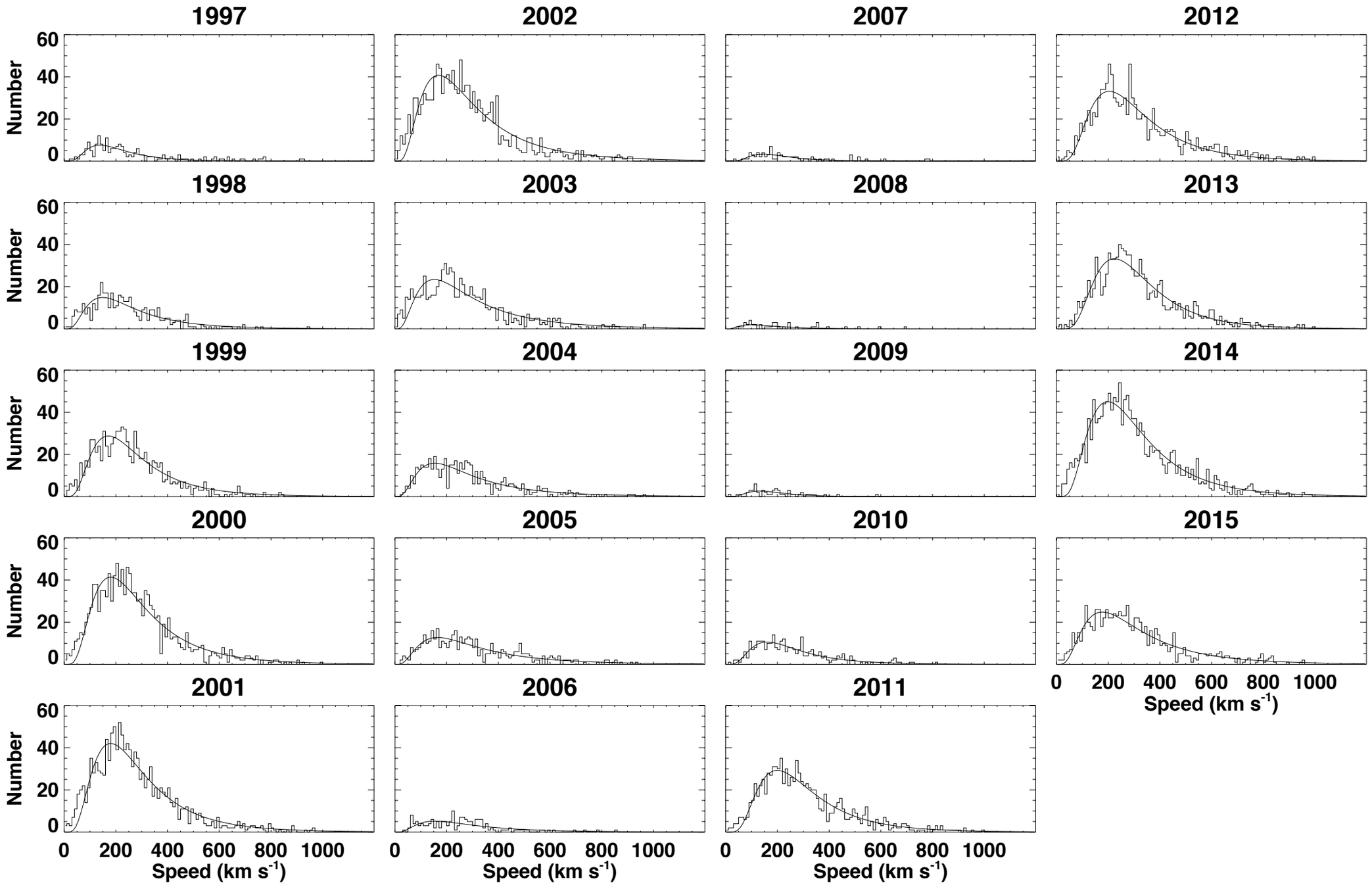

Annual histograms of CME velocity measurements from the SEEDS database. Fitted log-normal functions are overplotted.

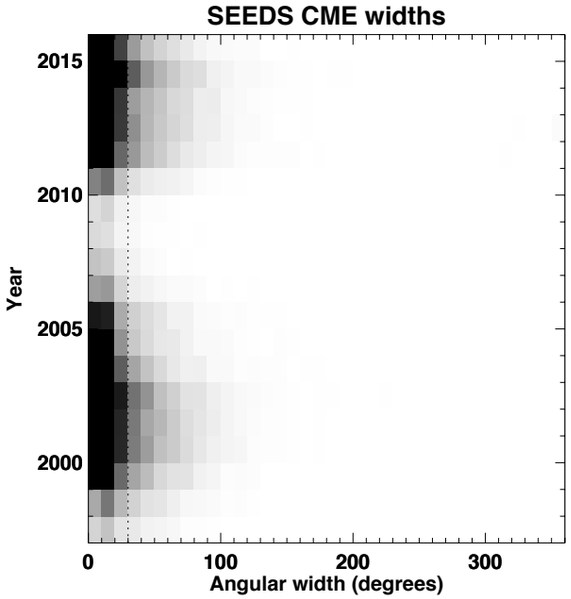

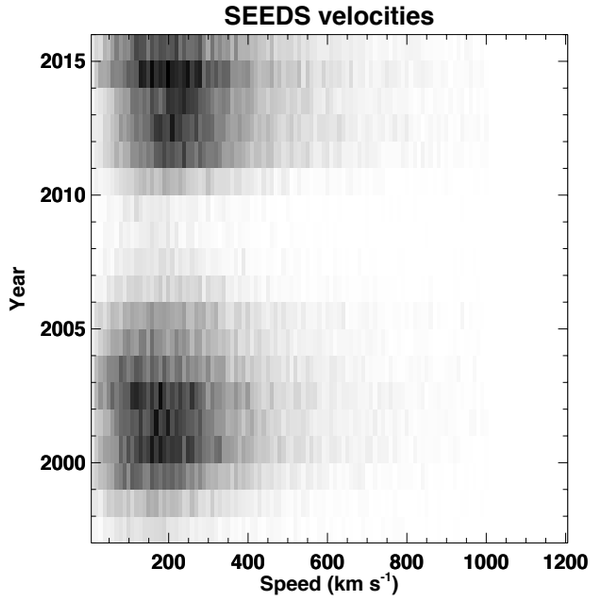

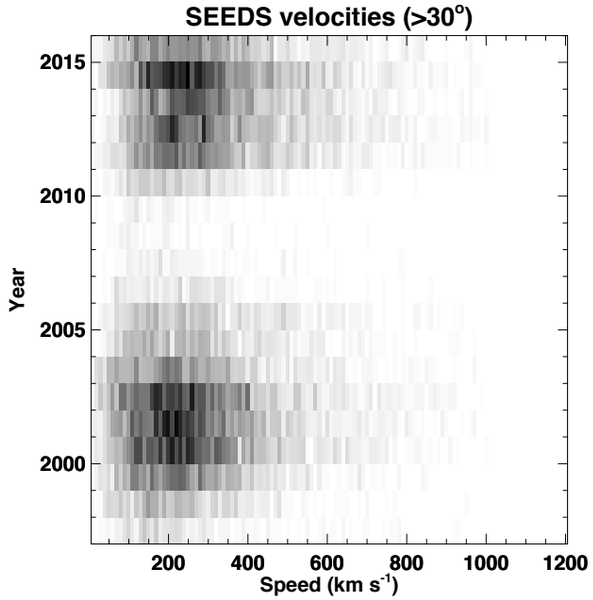

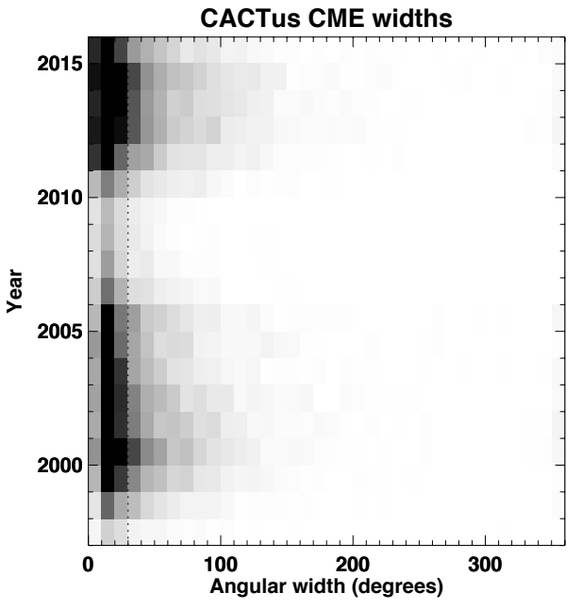

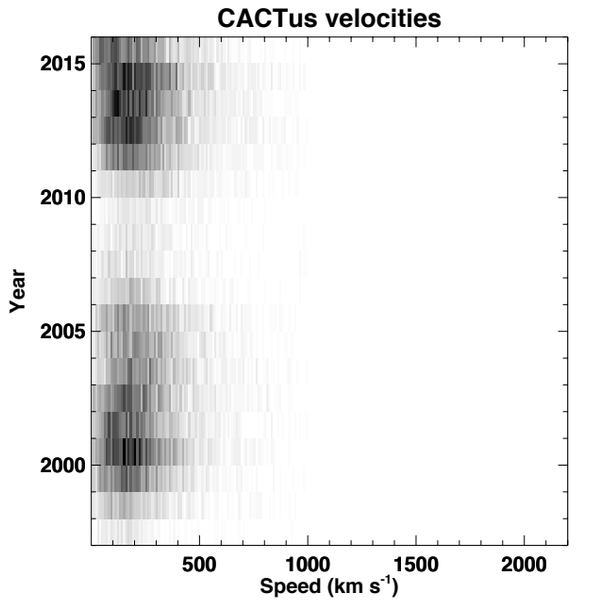

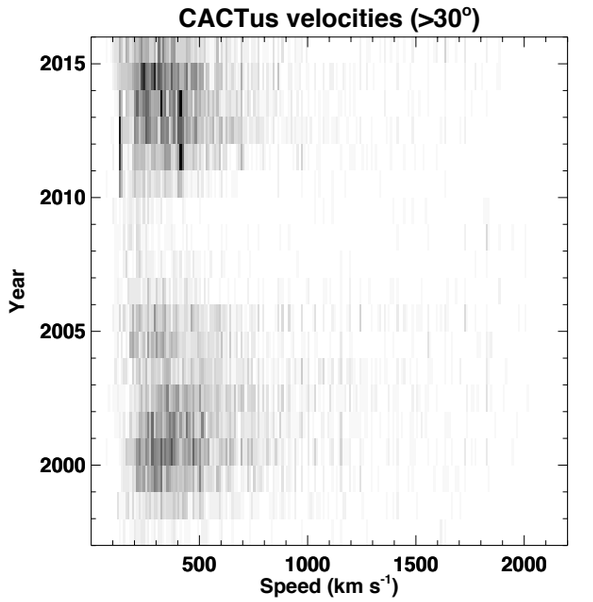

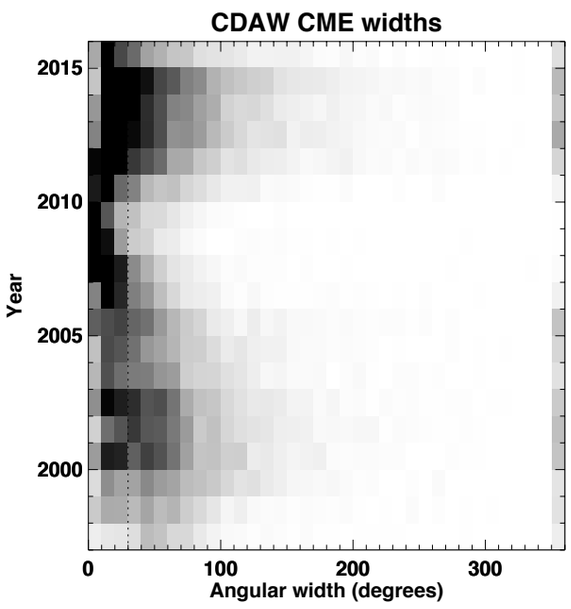

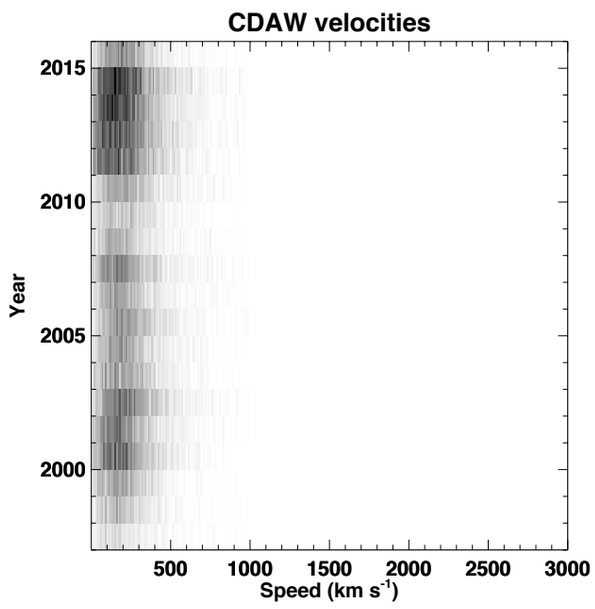

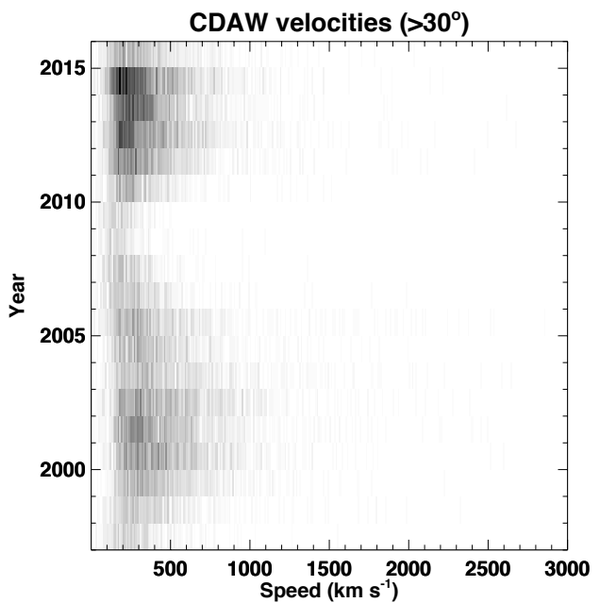

Stacked annual histograms of CME angular widths (left) and velocities for all detections (middle) and for detections with angular width > 30° (right), from the SEEDS (top), CACTus (middle) and CDAW (bottom) databases. The dotted lines in the left plots indicate the angular width cutoff at 30° below which the detections are excluded from the right plots.

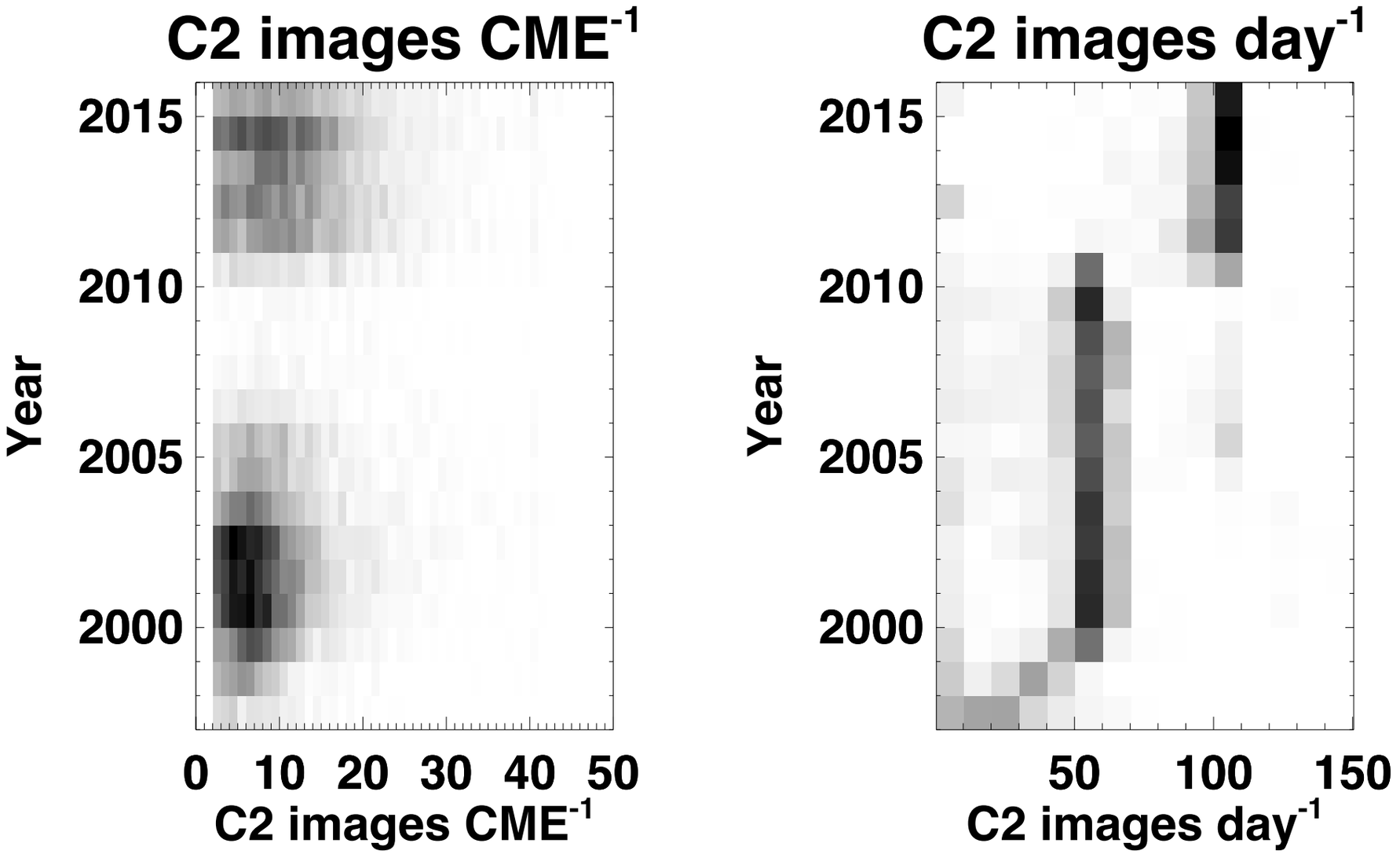

Main effect of LASCO image cadence change: more images per CME detection.

Stacked annual histograms of the number of LASCO C2 images per detected CME in the SEEDS database (left) and of the number of C2 images per day (right).

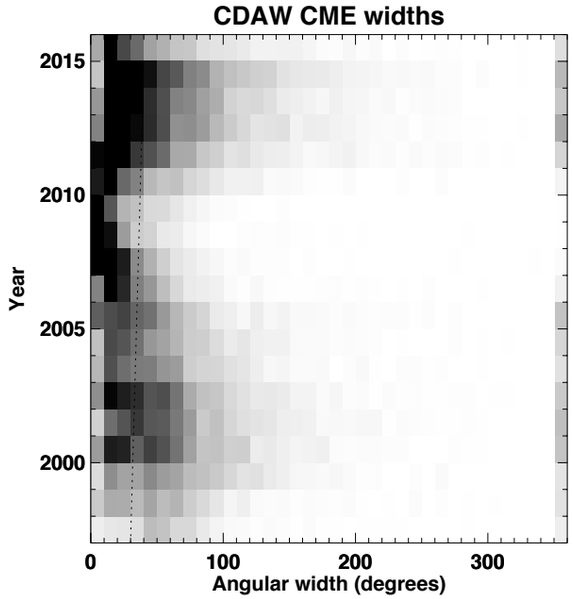

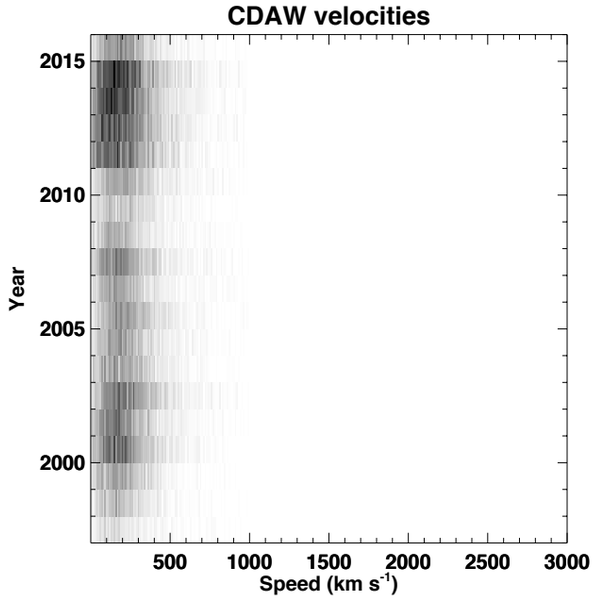

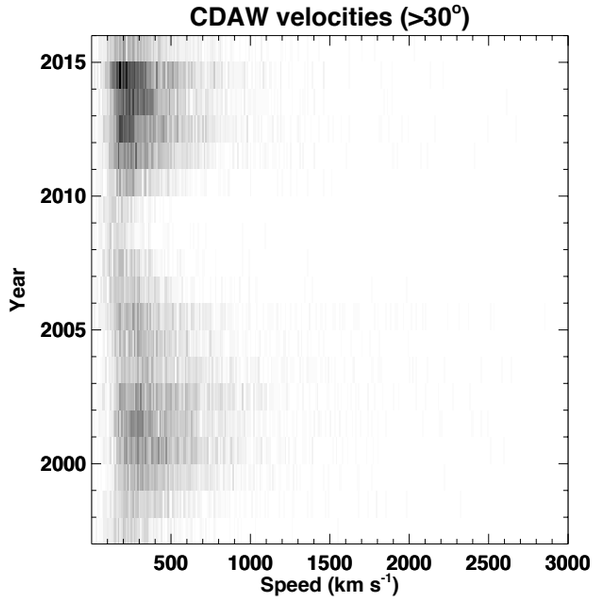

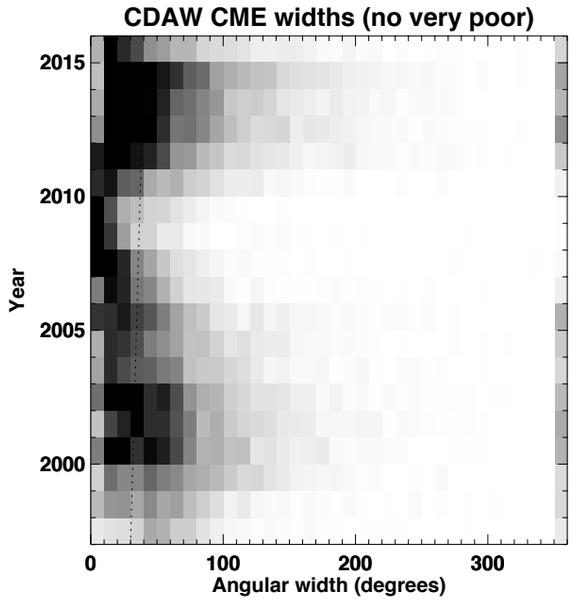

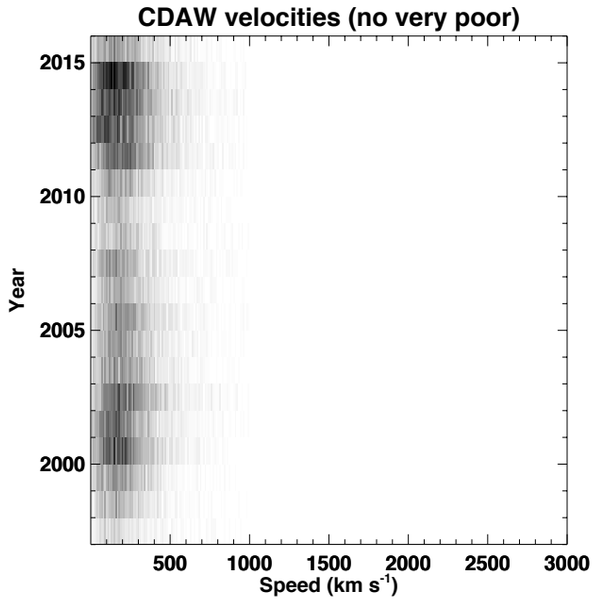

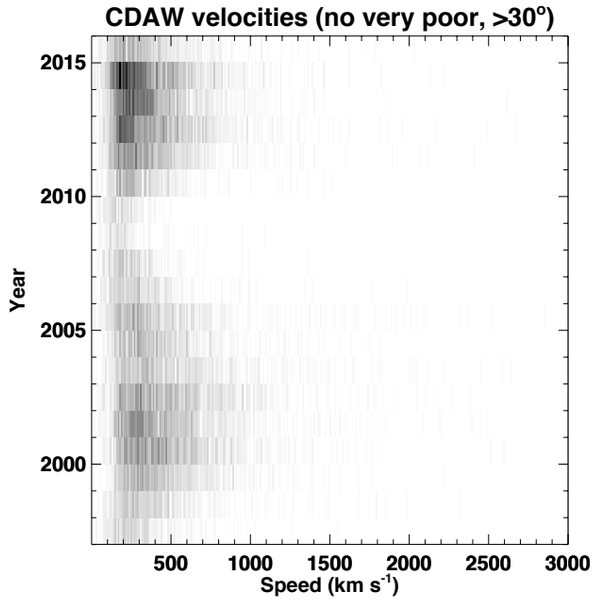

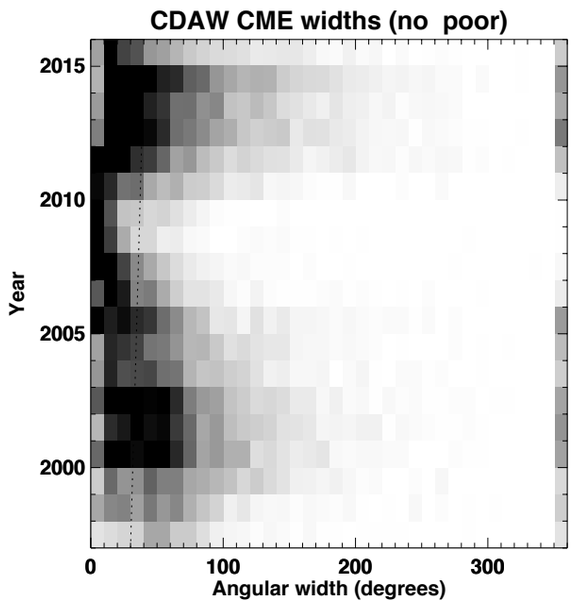

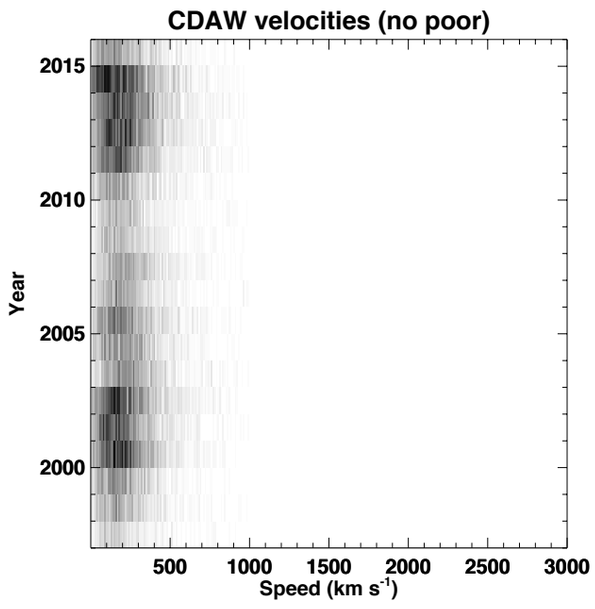

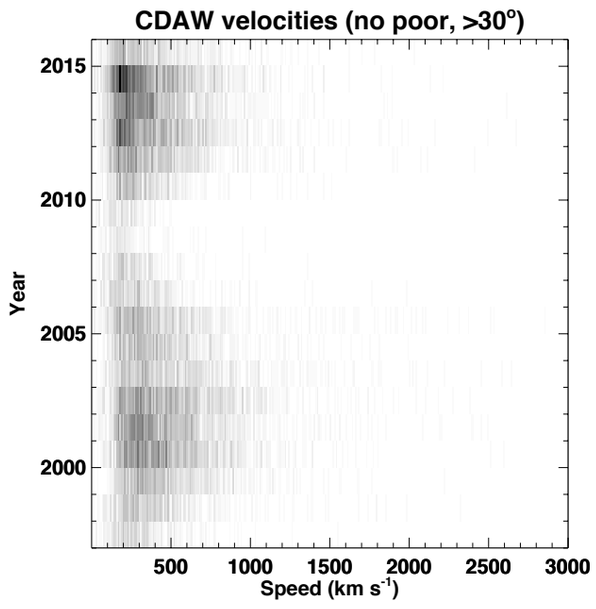

Stacked annual histograms of CME angular widths (left) and velocities for all detections (middle) and for detections with angular width > 30° (right), from the CDAW database.

All detections are included in the top plots, very poor detections are excluded from the middle plots, and poor and very poor detections are excluded from the bottom plots.

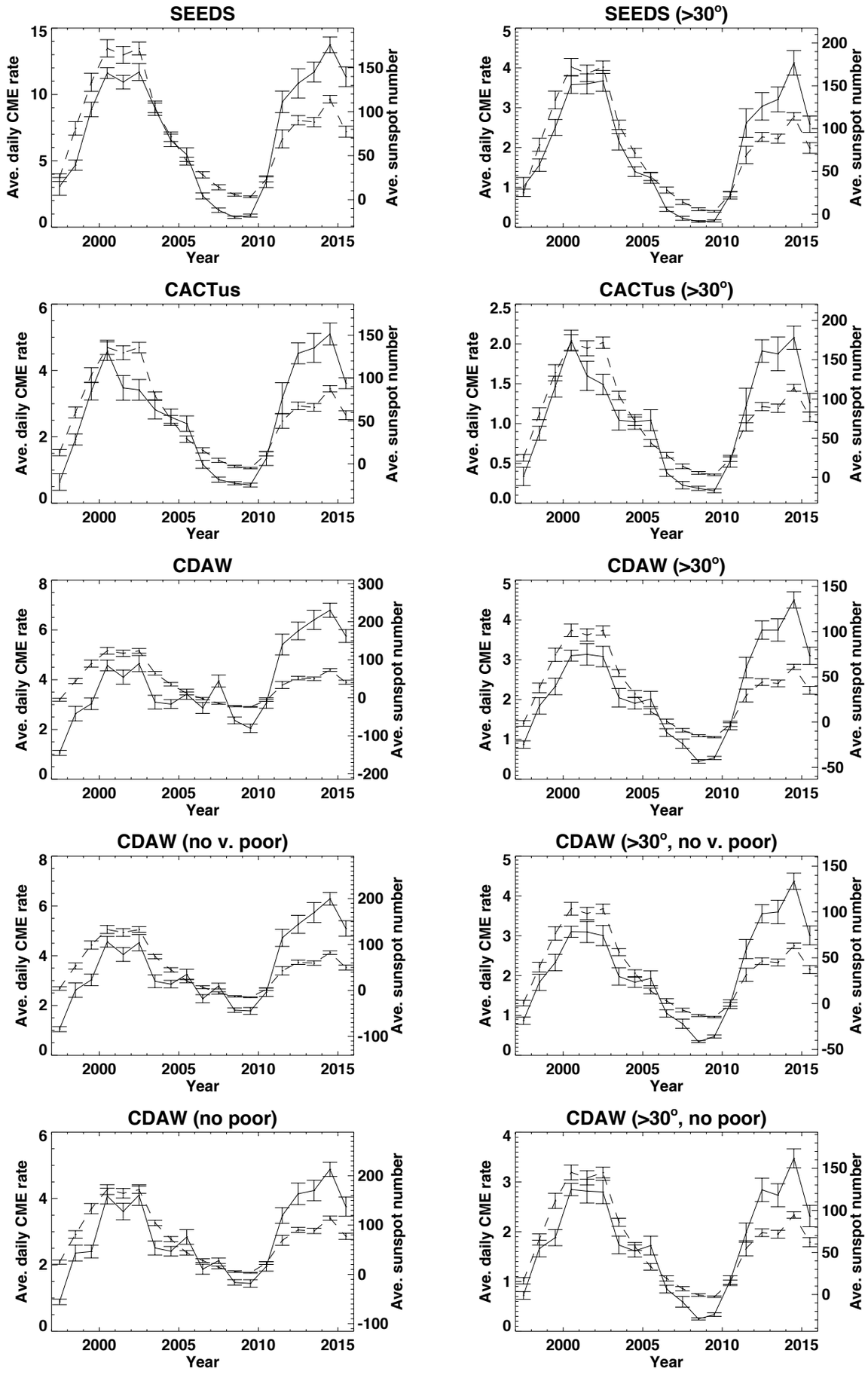

Average CME rates from SEEDS (top row), CACTus (second row) and CDAW (3rd-5th rows) with all cases included (3rd row), very poor cases excluded (4th row) and poor cases excluded (5th row).

In the right column only CMEs with angular width > 30° are included.

The average monthly sunspot number is overplotted in dashed curves for comparison.

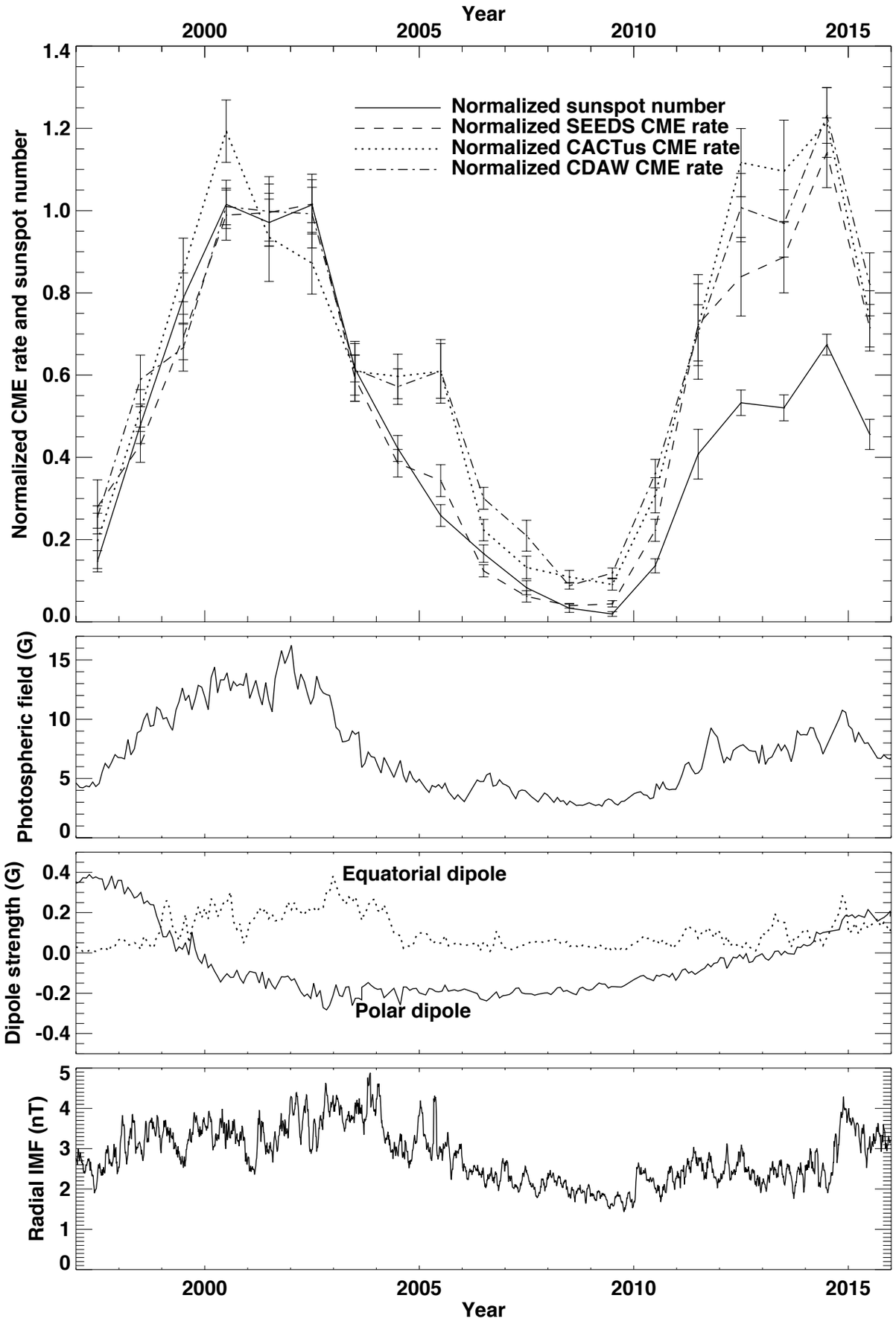

Normalized CME rates (top panel) from SEEDS, CACTus and CDAW including only detections with angular width > 30°, for the years 1997-2015. All poor and very poor cases have been excluded from the CDAW data. The normalized average monthly sunspot number is over-plotted in dashed curves. The CME rates have been normalized by their average values during the cycle 23 maximum years 2000-2002.

Second panel: total photospheric magnetic flux from NSO KPVT and SOLIS/VSM synoptic magnetograms.

Third panel: polar and equatorial dipole components of the same synoptic magnetograms.

Bottom panel: the OMNI 2 radial magnetic field component at 1 AU.

Summary

- In all three databases, SEEDS, CACTus and CDAW, a statistically significant increase in CME detections with angular width > 30° per sunspot number was found for cycle 24 compared to cycle 23.
- In the two databases based on both C2 and C3 images, CACTus and CDAW, the CME rate began to diverge from the sunspot number around 2004 after the polar field reversal. At nearly the same time, the IMF decreased by ≈ 30%.
- These results are consistent with the results of Gopalswamy et al. (2014, 2015), linking enhanced halo CME detections to increased CME expansion in a heliosphere of decreased total (magnetic+plasma) pressure.
- On the other hand, the SEEDS CME rate did not diverge from the sunspot number until the rise of cycle 24, in 2010-2011. This may be explained by the restriction of the SEEDS detections to the C2 field of view.
- The effect on these results of the 2010 LASCO image cadence changes is likely to have been small. They led mostly to a rise in images per detection and a decrease in low-quality detections, not enhanced detections of very fast or faint CMEs.
- Influence of the weakening of the solar magnetic field extends to CMEs.